Guest Investigator Report: Correcting Stray Light in SWAP

Paul Shearer

September 28, 2012

All telescope images suffer some degradation due to optical scattering. Extreme ultraviolet (EUV) images of the Sun are contaminated with a halo of *stray light* because a significant fraction of the Sun's brightness is scattered across the entire imaging plane. This haze reduces the contrast of the image, making bright regions appear dimmer and faint regions brighter than they really are. Scattering can be characterized and removed by determining the telescope point spread function (PSF). In this report, we determine SWAP's PSF and use it to remove the stray light haze from SWAP images. We also use the corrected images to identify and remove horizontal line artifacts observed at very low intensities.

Scattering in EUV telescopes is caused by non-specular reflection off of microrough mirror surfaces, as well as diffraction by the pupil and mesh grids or scintillators in the optical path. In SWAP, diffraction effects are very short-range, so we expect that mirror microroughness produces almost all stray light. Mirror surface irregularities produce a PSF with a narrow core but very broad and shallow wings. It is these wings which spread the thin layer of stray light across the image, but because they are so shallow, the Sun is the only known EUV source bright enough to make their contribution noticeable. Scattering from these sources is spatially invariant above the pixel scale, so stray light contamination is well-modeled by convolution of the unknown clean image with the PSF. Conversely, the clean image may be restored by *deconvolving* the PSF from the contaminated image [6], but the PSF must first be estimated using information from the images themselves.

The best information about the wings of EUV telescope PSFs comes from transit images of the Moon and the inner planets. These objects do not emit in the EUV, but EUV images of them contain scattered light from the Sun. DeForest et. al. were first to exploit this idea in [2], where they used a Venusian transit to fit a truncated Lorentzian model for the wings of the TRACE PSF. The PSFs for the four filter bands of EUVI-B, the EUV imager aboard STEREO-B, were determined by Shearer et. al. in [5] using a lunar transit. Shearer et. al. use a more sophisticated model of the PSF wings and they determine the uncontaminated image and the PSF simultaneously, which eliminates the need to guess the uncontaminated image as was done in [2]. For SWAP we adopt a slightly simplified version of the method in [5].

1 Blind Deconvolution Method

To obtain a PSF from the SWAP lunar transit, we first defined a simple but physically reasonable PSF model. Simplicity ensures that the fit is well-constrained by the available transit data and robust to non-stray light effects such as detector nonlinearity. We then determine best-fit values for the PSF parameters by solving a (semi-)blind deconvolution problem in which the lunar disk of the stray light corrected images is constrained to be zero.

1.1 PSF model

The PSF h is modeled using a slightly modified version of the microroughness PSF model in [5]. We assume that a fraction α of light is not scattered, giving the PSF a single-pixel core with mass α. The remaining fraction $1-\alpha$ is scattered according to a power law with a decay rate β, which may depend on the distance r from the PSF origin. To model anisotropy, the isotropic profile is stretched in one direction, transforming its circular level sets into ellipses. The resulting PSF model accommodates anisotropy and irregular wing decay with just a few parameters.

We use this model because it is mathematically convenient and a physically reasonable model of microrough mirror scatter. For microrough mirror PSFs, the wings are described by the power spectral density (PSD) of the mirror surface height function, and this PSD has been directly measured [4]. A log-log plot of the measured PSD versus spatial frequency is roughly piecewise linear, and making this assumption explicitly leads directly to our proposed model. Deconvolution with a PSF from this model is especially easy, because when $\alpha > 1/2$ the matrix that performs the convolution operation is diagonally dominant and hence stably invertible.

To represent the variable exponent power law mathematically, we define a series of logarithmically spaced breakpoints $1 = r_0 < r_1 < r_2 < \ldots < r_b = r_{max}$, where r_{max} is the length of the image diagonal in pixels, and define β_i the decay exponent on the interval $[r_{i-1}, r_i)$. The number of intervals b was set to 7, close to the value in [5]. The initial isotropic PSF profile $p_{\alpha,\boldsymbol{\beta}}(r)$ is then given by

$$p_{\alpha,\boldsymbol{\beta}}(r) = \begin{cases} \alpha & \text{if } r = 0 \\ (1-\alpha)c_i r^{-\beta_i}, & \text{if } r \in [r_{i-1}, r_i) \end{cases}, \tag{1}$$

where the c_i are determined by the condition that the pieces must link together continuously. Note that if a logarithm is applied to both sides, then $\log p$ is a continuous piecewise linear function of $\log r$, so the profile can be generated on a computer by fitting a spline in log-log space and applying an exponential. The isotropic PSF generated from this profile can be written as $p_{\alpha,\boldsymbol{\beta}}(\|x\|_2)$, where $x \in \mathbb{R}^2$.

To stretch the isotropic PSF, we define s to be the stretch factor and θ the CCW angle in radians between the stretch axis and the horizontal. We apply a horizontal stretch by a factor of s and a rotation by θ radians to the graph of $p_{\alpha,\boldsymbol{\beta}}(\|x\|_2)$. This graph transformation

can be implemented by applying its inverse directly to x:

$$h_\varphi(x) = C \cdot p_{\alpha,\boldsymbol{\beta}}(\|M_{s,\theta}^{-1} \cdot x\|_2), \quad \text{where} \tag{2}$$

$$M_{s,\theta} = \begin{bmatrix} \cos(\theta) & \sin(-\theta) \\ \sin(\theta) & \cos(\theta) \end{bmatrix} \begin{bmatrix} s & 0 \\ 0 & 1 \end{bmatrix}. \tag{3}$$

Here C is the normalizing constant defined to make the PSF sum to unity.

1.2 Fitting Method

To determine the PSF from N lunar transit images $f_1, \ldots, f_N$, we must solve for the PSF parameters φ and the clean lunar transit images $u_1, \ldots, u_N$ simultaneously. We require that each u_i must be zero on the set of lunar disk pixels Z_i, and the PSF h_φ and the u_i must convolve together to form the f_i. This gives a large constrained nonlinear system of equations which we will solve in the least squares sense:

$$\begin{aligned} f_1 &= h_\varphi * u_1, \quad u_1(Z_1) = 0 \\ f_2 &= h_\varphi * u_2, \quad u_2(Z_2) = 0 \\ &\cdots \\ f_N &= h_\varphi * u_N, \quad u_N(Z_N) = 0, \end{aligned} \tag{4}$$

where

$$(u * v)(x) = \sum_{x' \in I} u(x - x')v(x') \tag{5}$$

denotes the convolution of two arrays u and v over the index set I of the 1024×1024 pixel array of CMOS detectors in SWAP. (We use zero boundary conditions, setting $u(x - x') = 0$ at pixels $x - x' \notin I$.) The least squares optimization problem may be written as

$$\begin{aligned} \underset{\varphi=(\boldsymbol{\beta},\alpha,s,\theta),\ \{u_i\}}{\text{minimize}} \quad & \sum_{i=1}^{N} \|h_\varphi * u_i - f_i\|^2 \\ \text{subject to} \quad & u_i(Z_i) = 0 \text{ for all } i, \\ & \boldsymbol{\beta} \geq 0,\ 0 \leq \alpha \leq 1. \end{aligned} \tag{6}$$

Since each u_i is a 1024×1024 image, this problem has over N million free variables and is difficult to solve by general-purpose numerical methods. However, if φ is set to some fixed value and the zero variables $u_i(Z_i)$ are eliminated, it decomposes into N separate unconstrained linear least squares problems, each of which is easily solved by a few iterations of the conjugate gradient method. If we write the solution to each linear problem as $(u_i)_\varphi$, the problem reduces to

$$\begin{aligned} \underset{\varphi=(\boldsymbol{\beta},\alpha,s,\theta)}{\text{minimize}} \quad & \sum_{i=1}^{N} \|h_\varphi * (u_i)_\varphi - f_i\|^2 \\ \text{subject to} \quad & \boldsymbol{\beta} \geq 0,\ 0 \leq \alpha \leq 1, \end{aligned} \tag{7}$$

which has $b + 3 = 10$ free variables and is much more tractable. This problem can be solved by any reasonable nonlinear least squares optimizer; we used MATLAB's `lsqnonlin` function. We chose $N = 6$ images from an eclipse observed by SWAP on June 1, 2011 and obtained the PSF shown in Fig. 1.

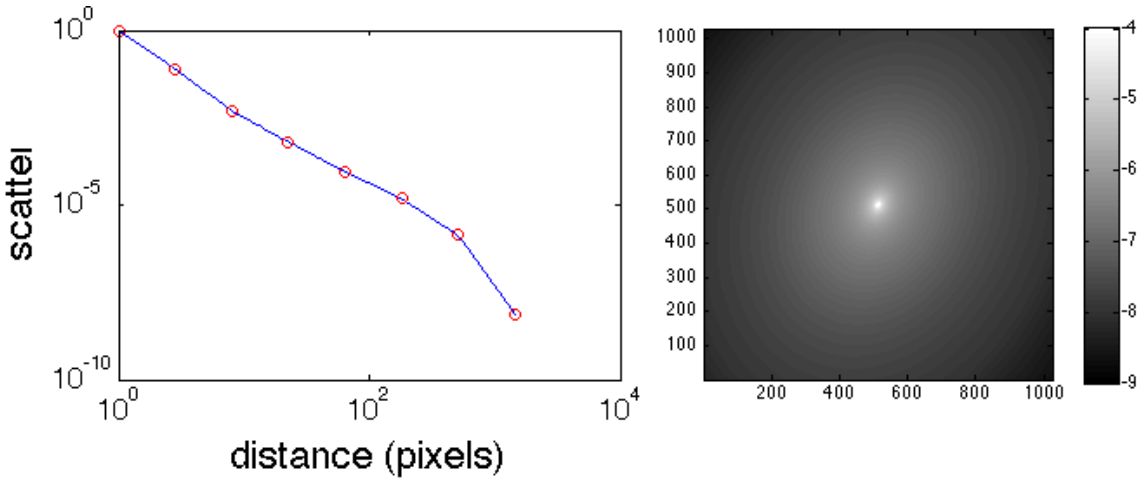

Figure 1: An overview of the 171 Å PSF structure. All distances are in pixels. *Left:* log-log plot of power-law profile function $p_{\alpha,\beta}(r)$ with breakpoints marked. *Right:* final anisotropic PSF h_φ (logarithmic scale).

1.3 Validation and Results

Using our PSF, any SWAP image f can be corrected by a fast Fourier domain deconvolution. We pad both the image f and the PSF h to twice their size with zeros, compute the Fourier transforms $\hat{f}$ and $\hat{h}$, take the inverse Fourier transform of the quotient $\hat{f}/\hat{h}$, then remove the padding. (As we mentioned above, there is no need for regularization because $\hat{h}$ never approaches zero.) This algorithm takes less than a second to deconvolve a SWAP image and is practically indistinguishable from the more computationally intensive conjugate gradient method used in [5], although the latter may be more accurate if significant signal exists near the image boundary.

One simple validation is to see whether the deconvolution makes sense on lunar transit images, particularly ones that were not used to fit the PSF. Deconvolution with a correct PSF will make the lunar disk zero and not produce any substantial violations of positivity. In Fig. 2 we see that this is indeed the case.

In another validation similar to [5], the direction and magnitude of the anisotropy was independently confirmed by comparing SWAP images taken at different spacecraft orientations. Since stray light is instrumental in origin, it appears to move with the solar image if the spacecraft is rotated. This phenomenon is most apparent if the difference between two Sun-aligned images is taken: such difference images exhibit a light axis and a dark axis in the off-limb, indicating the dominant direction of scatter in each image (Fig. 3, left). Deconvolving images with our PSF greatly reduces these axes (right).

2 Horizontal line artifact removal

Removing stray light enabled us to correct another instrument issue that was previously entangled with it. At very low intensities near the digital number (DN) readout limit of the

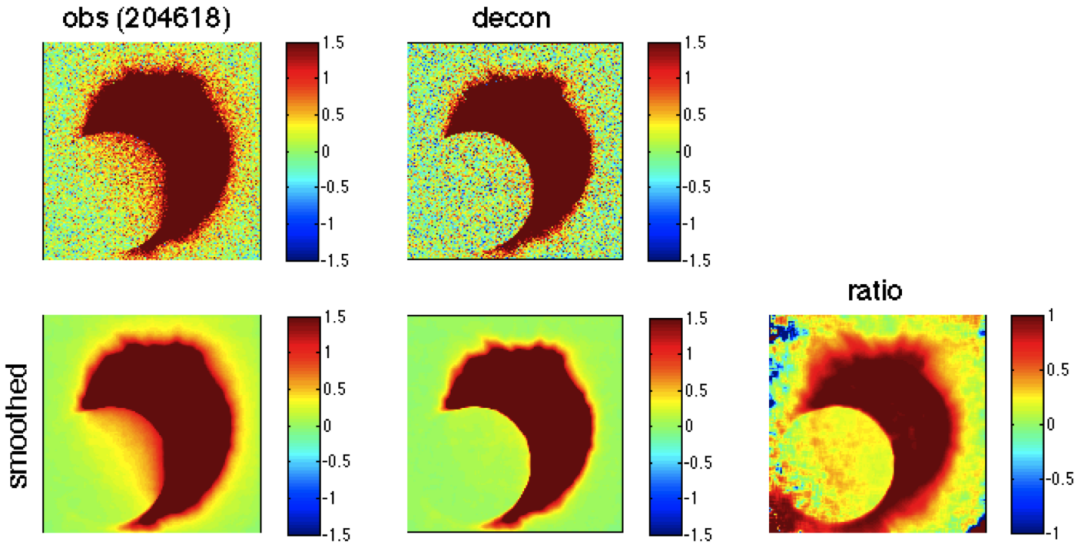

Figure 2: Comparison of lunar eclipse images before stray light correction (*left column*) and after (*middle column*) with units of DN. The colorbar has a very low upper limit and is symmetric around zero to make stray light and positivity violations easy to see. In the bottom row, the images are smoothed with a 32×32 boxcar to reduce noise. In the right column, the ratio deconvolved/observed of the smoothed images is shown. A ghost of the solar limb is visible in the ratio, which is due to the changing and nonlinear response of the CMOS detector.

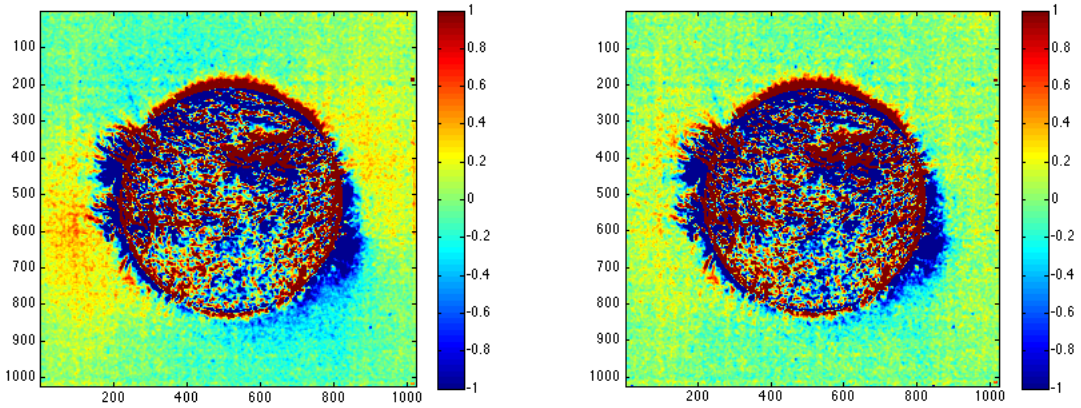

Figure 3: Difference of Sun-aligned roll images before stray light correction (*left*) and after (*right*), units of DN. An 8×8 boxcar was applied to make the large-scale stray light distribution visible above the image noise.

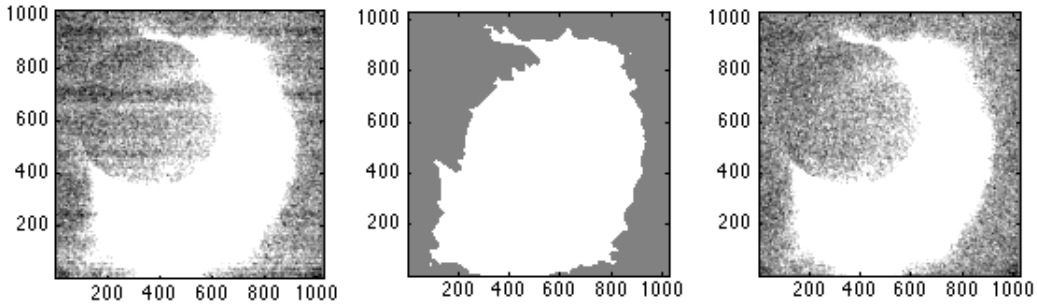

Figure 4: SWAP horizontal line removal. *Left:* a lunar transit image before horizontal line removal. The color scale ranges from -0.2 to 0.2 DN, and a 10×10 median filter was applied to make the lines clearly visible above the noise. *Center:* the mask derived from thresholding this image (*center*), and the image after removing the median value of the non-masked pixels in each row (*right*).

detector, SWAP images suffer from additive horizontal line artifacts caused by nonuniformities in the detector readout process. After performing stray light correction, we observed that these artifacts could be separated from the solar image, whereas before they were difficult to distinguish from the stray light halo.

Fig. 4, *left*, shows a deconvolved SWAP lunar transit image which has been median filtered to make the horizontal line artifacts more prominent. To remove the lines, we median filter the rows of the image, excluding any pixels that may contain solar signal. An initial pixel exclusion mask is defined by including any pixels above a certain threshold and any pixels inside the solar disk; a neighborhood filter is then used to make this initial mask more conservative. The mask derived for the lunar transit image is shown in the middle of Fig. 4. After we take the median across each row of the masked image, we subtract it off from each row. To avoid confusing interactions with dark current and other corrections, we require that the overall correction be centered around zero. To accomplish this, we add the median of the unmasked pixels back into the row-corrected image. The final result is given in Fig. 4, *right*, where the lines have clearly disappeared. Note that a ghost of the solar limb is difficult to make out in the uncorrected image, but is clearly visible in the corrected one.

References

[1] J. C. Brown, B. N. Dwivedi, et al. The interpretation of density sensitive line diagnostics from inhomogeneous plasmas. ii - non-isothermal plasmas. *Astronomy and Astrophysics*, 249(1):277, 1991.

[2] C. E. DeForest, P. C. H. Martens, and M. J. Wills-Davey. Solar coronal structure and stray light in trace. *The Astrophysical Journal*, 690(2):1264, 2009.

[3] R. A. Frazin, A. M. Vásquez, and F. Kamalabadi. Quantitative, three-dimensional analysis of the global corona with multi-spacecraft differential emission measure tomography. *The Astrophysical Journal*, 701:547–560, 2009.

[4] Dennis Martínez-Galarce, James Harvey, et al. A novel forward-model technique for estimating euv imaging performance: design and analysis of the suvi telescope. *Proc. SPIE*, 7732(1):773237, 2010.

[5] P. Shearer, R. A. Frazin, et al. The First Stray Light Corrected EUV Images of Solar Coronal Holes. *ArXiv e-prints*, October 2011.

[6] J. L. Starck, E. Pantin, and F. Murtagh. Deconvolution in astronomy: A review. *PASP*, 114(800):1051–1069, 2002.